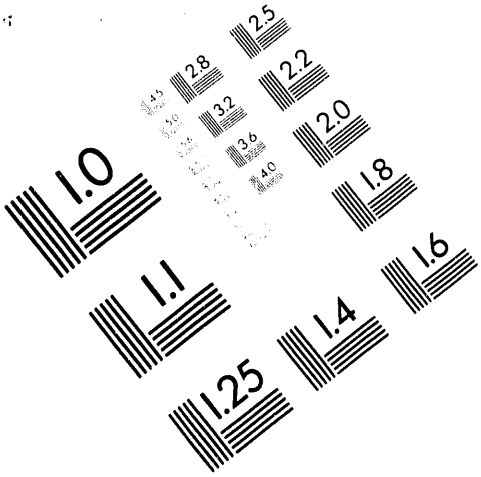

Association for Information and Image Management

1100 Wayne Avenue, Suite 1100
Silver Spring, Maryland 20910

301/587-8202

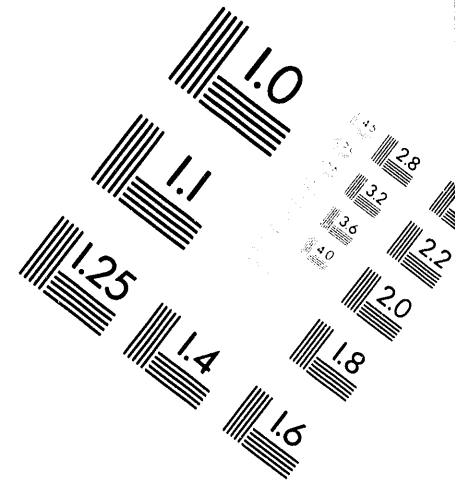

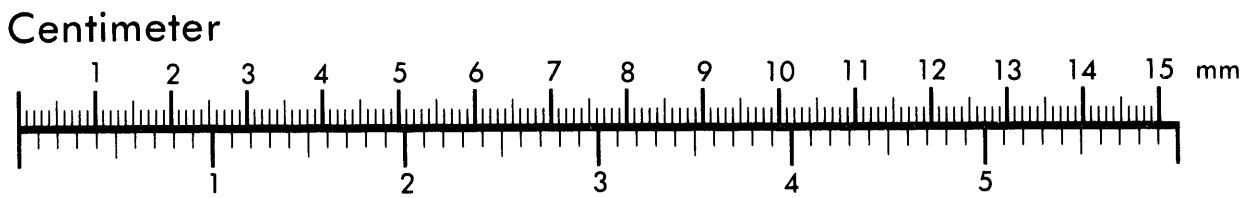

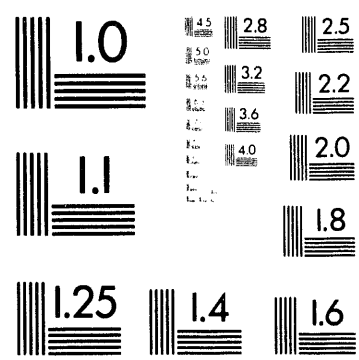

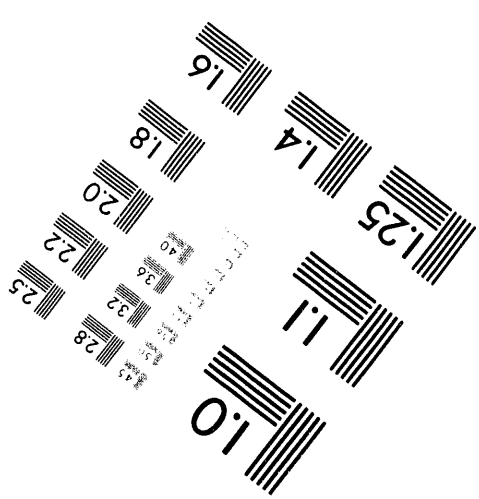

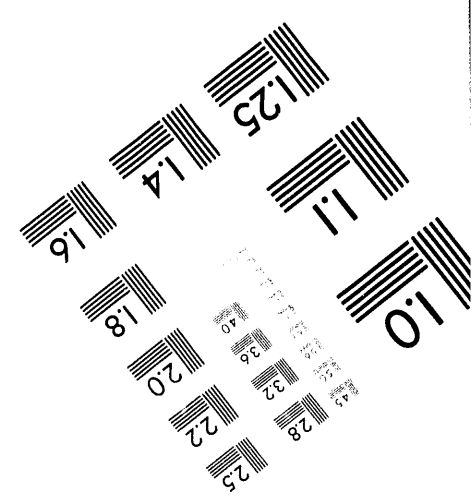

MANUFACTURED TO AIIM STANDARDS
BY APPLIED IMAGE, INC.

1 of 1

DOE/AL62353-2

SPARK IGNITED TURBULENT FLAME KERNEL GROWTH

Annual Report for the Period
January-December 1992

Domenic A. Santavicca

PENN STATE UNIVERSITY
University Park, PA 16802

Date Published - June 1994

PREPARED FOR THE UNITED STATES
DEPARTMENT OF ENERGY

Under Contract No. DE-FG04-90AL62353

ABSTRACT

Results from an experimental study of the effect of incomplete fuel-air mixing on spark-ignited flame kernel growth in turbulent propane-air mixtures are presented. The experiments were conducted in a turbulent flow system that allows for independent variation of flow parameters, ignition system parameters, and the degree of fuel-air mixing. Measurements were made at 1 atm and 300 K conditions. Five cases were studied; a premixed and four incompletely mixed cases with 6%, 13%, 24% and 33% RMS (root-mean-square) fluctuations in the fuel/air equivalence ratio. The overall fuel/air equivalence ratio was unity in all cases. The flow characteristics were measured by LDV. The RMS fluctuation in the fuel/air equivalence ratio was characterized using NO_2-based laser induced fluorescence. High speed laser shadowgraphy at 4,000 frames-per-second was used to record flame kernel growth following spark ignition, from which the equivalent flame kernel radius as a function of time was determined. The effect of incomplete fuel-air mixing was evaluated in terms of the flame kernel growth rate, "cyclic" variations in the flame kernel growth, and the rate of misfire.

The results show that fluctuations in local mixture strength due to incomplete fuel-air mixing cause the flame kernel surface to become wrinkled and distorted; and that the amount of wrinkling increases as the degree of incomplete fuel-air mixing increases. Incomplete fuel-air mixing was also found to result in a significant increase in "cyclic" variations in the flame kernel growth. The average flame kernel growth rates for the premixed and the incompletely mixed cases were found to be within the experimental uncertainty except for the 33%-RMS-fluctuation case where the growth rate is significantly lower. The premixed and 6%-RMS-fluctuation cases had a 0% misfire rate. The misfire rates were 1% and 2% for the 13%-RMS-fluctuation and 24%-RMS-fluctuation cases, respectively; however, it drastically increased to 23% in the 33%-RMS-fluctuation case.

INTRODUCTION

Cyclic combustion variations in spark-ignition engines, which cause engine roughness and increased unburned hydrocarbon emissions, limit the use of dilute charge strategies for achieving low NOx emissions and improved fuel economy [1,2]. In spark-ignition engines, ignition and early flame-kernel growth are intimately related to the problem of cyclic variations in combustion [2]. Numerous efforts have been made to understand the effects of ignition system parameters [3-17] and flow field parameters [3, 7-10, 16, 18] on early flame kernel growth. In addition, mixture nonhomogeneity resulting from incomplete mixing of fuel and air (and residual or exhaust gases), may also have a significant impact on early flame kernel growth. Mixture nonhomogeneity is likely to be a major factor contributing to cyclic combustion variations in current port injected spark ignition engines, especially under cold start conditions. A better understanding of spark-ignited flame-kernel growth in nonhomogeneous charges is essential for the development of improved spark-ignition engines. Several investigations have been conducted of the effects of mixture nonhomogeneity on engine combustion. The results of these studies are summarized below.

In 1978, Peters and Quader [19] demonstrated the effect of fuel-air mixture preparation on the lean operation of a single-cylinder spark ignition engine. Mixture preparation was changed by varying the time of fuel injection into the intake manifold. They found that the use of a premixed charge resulted in a richer lean misfire limit, lower maximum burning rate, higher hydrocarbon emissions, and increased ISFC relative to an apparently heterogeneous mixture. Therefore some form of heterogeneous intake charge "wetted" with fuel droplets and possibly with bulk stratification was found to be beneficial for lean combustion.

In 1981, Pundir et al. [20] demonstrated the influence of charge nonhomogeneity on cycle-to-cycle combustion variations in a single-cylinder, variable compression ratio CFR engine. Various degrees of charge nonhomogeneity were obtained with propane and gasoline using a plain valve or a shrouded valve. Charge nonhomogeneity was determined from exhaust gas analysis. The results showed that cyclic variations in maximum combustion pressure increase with an increase in charge nonhomogeneity at a given mixture strength. For the same charge nonhomogeneity, cyclic variations also increase with leaner fuel-air mixtures and with increasing duration of the initial phase of combustion.

In 1990, Kajitani et al. [21] investigated engine combustion behavior when the mixture condition at the intake port was varied by changing the portions of atomized liquid fuel and fully vaporized fuel in the mixture. A single cylinder, four cycle, side valve engine was used. The experiments were conducted with various amounts of atomized fuel but at a fixed fuel/air equivalence ratio of 1.0. When the mixture at the intake port contained about 30% atomized liquid fuel, the engine exhibited the highest mean effective pressure and thermal efficiency. The combustion deteriorated with 40% or more atomized liquid fuel. Late MBT spark timing was needed for mixtures with higher amounts of atomized fuel, which was attributed to faster flame propagation at the early stages of combustion. Cyclic variations in peak pressure were greater with mixtures containing some atomized fuel.

In 1990, Sztenderowicz and Heywood [22] studied cycle-to-cycle combustion variability in a single cylinder research engine (Ricardo Hydra Mk III) and how it is influenced by spatial nonhomogeneity in the unburned mixture. They chose two mixture-nonhomogeneity cases: a typical nonhomogeneous mixture obtained with port fuel injection of indolene, and a perfect mixture of premixed isooctane prepared in a mixing tank before entering the combustion chamber. The overall fuel/air equivalence ratio was fixed at 1.0 for both cases. Exhaust gas analysis revealed that fuel/air nonhomogeneity was roughly cut in half when fuel injection with indolene was replaced by premixed isooctane. The reduction in mixture nonhomogeneity was accompanied by a slight reduction in the standard deviation of flame initiation and development angles $\theta_{0\text{-}2\%}$ and $\theta_{0\text{-}10\%}$. However, no significant impact was revealed in the statistics of the main combustion phase $\theta_{10\text{-}90\%}$.

In 1991, Daniels et al. [23] developed an experimental technique for evaluating the influence of mixture preparation on the performance of a spark ignition engine. The preparation components investigated were fuel vapor, droplets, and liquid streams. Their effects on cylinder pressure and exhaust gas concentration were studied in a production engine. The results showed that the performance (IMEP, exhaust emissions, etc.) of the engine was diminished by increasing the amount of fuel in liquid-stream form, which was believed to result in the greatest mixture nonhomogeneity.

Although these studies show that the method of mixture preparation can have a significant impact on engine combustion, the degree to which mixture nonhomogeneity contributes to cyclic combustion variations is still not well understood. The relationship between incomplete fuel-air mixing and cyclic combustion variability in engines has been difficult to resolve in an actual engine due to the difficulties of controlling and quantifying the degree of incomplete fuel-air mixing in an engine combustion chamber. Recently, several non-intrusive laser-based measurement techniques which quantify the spatial and temporal nonhomogeneity of fuel-air mixtures in SI engine combustion chambers have been developed. These include an NO_2-based laser-induced fluorescence (LIF) technique [24], a laser Rayleigh scattering technique [25-28], a 2-D LIF technique [29,30], and a 2-D laser induced exciplex fluorescence (LIEF) technique [31]. Although the application of such techniques to realistic engine systems has been limited to date, valuable information on typical levels of mixture nonhomogeneity has been obtained. For example, the results reported by Baritaud and Heinze in 1992 [29] showed that 15 - 20% root-mean-square (RMS) fluctuations in the fuel/air equivalence ratio at 25° BTDC were observed using a biacetyl-based 2-D LIF technique in a single cylinder engine with optical access. In 1992, Maly et al. [30] used an ethylmethylketon-based 2-D LIF technique in a transparent square piston engine, and reported that the fluctuation in the excess air ratio was 0.8 - 1.2 at 40° BTDC.

In order to study the effects of incomplete fuel-air mixing on early flame-kernel growth and cyclic variations in combustion, the experiments reported in this paper were conducted in a turbulent flow system designed to create the desired degree of incomplete fuel-air mixing in a well-controlled flow field. The NO_2-based LIF technique was used to characterize mixture nonhomogeneity in the test section, and laser Doppler velocimetry (LDV) was used to characterize the turbulent flow field. Growth of spark-ignited flame kernels was measured by means of high-speed laser shadowgraphy to gather information about the equivalent flame kernel radius and its growth rate versus time. The effect of incomplete fuel-air mixing on flame kernel growth, "cyclic" variations, and misfire rate are presented and discussed.

EXPERIMENT

TURBULENT FLOW SYSTEM - The turbulent flow system illustrated in Fig. 1 was designed to allow independent variation of the mean velocity and turbulence intensity, as well as, the degree of fuel-air mixing in the

test section. Turbulence is generated by forcing the primary flow through two narrow slots (0.32 mm wide by 50.8 mm long) in the slot plate, as illustrated in Fig. 1. This produces large vortices which then breakup in a converging section before entering the test section, resulting in very high levels of homogeneous, isotropic turbulence [32]. The mean velocity and turbulence intensity were measured with LDV at nine locations over the width of the test section, at the same height as the spark electrode. The measured flow characteristics are shown in Fig. 2. The mean velocity and turbulence intensity averaged over the nine locations were 1.16 m/sec and 0.25 m/sec, respectively. Relative to the flow conditions in an engine, the turbulence level corresponds to a ratio of turbulence intensity to mean piston speed (for a 10 cm stroke and 800 rpm) of ~ 1/10. The integral length scale was estimated to be 4 mm, based on two-point spatial correlation measurements made in a nearly identical flow system [32].

Incomplete fuel-air mixing is achieved by introducing the fuel (propane) at two different locations. The primary location is about 160 flow tube diameters upstream of the test section which insures complete fuel-air mixing. The secondary location is approximately 1 cm upstream of the test section where the fuel is introduced through four fuel tubes, as shown in Fig. 1. By varying the fraction of fuel added at these two locations, the degree of incomplete fuel-air mixing in the test section can be changed. In this study, a (100%) premixed case and four incompletely mixed cases were established while the overall fuel-to-air (fuel/air) equivalence ratio was 1.0. These four cases are referred to as the 75% premixed, 50% premixed, 25% premixed, and 0% prer xed cases. For example, the 75% premixed case is obtained by adding 75% of the fuel at the primary location and the 25% at the secondary location. By selecting the size of the fuel tubes so that the mean gas velocity of the secondary fuel jets matches the mean velocity of the primary flow, the secondary fuel was introduced without appreciably changing the turbulence properties of the primary flow. This was confirmed by making LDV measurements with and without the secondary fuel flow while maintaining the same flow rate through the test section.

NO_2-BASED LIF TECHNIQUE - The degree of fuel-air mixing was characterized using an NO_2-based LIF technique. This technique involves replacing the fuel with an equivalent volume flow rate of nitrogen which is doped with 6500 ppm of NO_2. It is assumed that the NO_2 mixes well with air at a molecular level and that it tracks all time and length scales in the flow of interest to yield accurate information about the fluctuations in fuel concentration. The major drawback in using NO_2 is that it is highly toxic, necessitating extreme caution during its use. NO_2 absorbs radiation over a relatively broad band of wavelengths with many lines in the visible spectrum that are easily accessible with an argon-ion laser, and subsequently emits broad band radiation at longer wavelengths [33, 24]. The intensity of the red-shifted fluorescence is proportional to the NO_2 concentration and therefore provides a measure of the instantaneous and local fuel to air ratio. A high signal to noise ratio may be achieved by using a long-pass filter to eliminate stray laser light scattered from windows, walls, etc..

A schematic diagram of the LIF setup is shown in Fig. 3. The 488 nm output of an argon-ion laser was used to excite the NO_2. The laser beam was focused with a 250 mm-focal length lens. The fluorescence signal was collected at 90 degree with a 121 mm-focal length, 60 mm diameter lens, and collimated by positioning the lens one focal length away from the probe volume. The collimated beam was then focused onto a 1.6 mm-diameter aperture using a second 121 mm-focal length lens, passed through a 515 nm-long pass filter to eliminate resonant scattering, and detected with a photomultiplier tube (PMT). Because the magnification ratio of the collection optics was 1:1, the spatial resolution was determined by the aperture size. The signal from the PMT was monitored and recorded by a digital oscilloscope and a computer based A/D system, respectively. All test section walls were painted black to reduce laser light reflection off the walls. The test section and all optical components were covered by a black-painted box to shield them from room lights and minimize background noise.

In the following, background noise is defined as the signal measured with no NO_2 and is primarily due to the small but finite transmissivity of the long-pass filter at the laser beam wavelength. Although it is impossible to remove the background noise completely, it must be minimized to achieve a high signal-to-noise ratio for accurate measurements. In order to determine a PMT input voltage yielding a highest signal-to-noise ratio, the signal and noise characteristics at various PMT input voltages were examined. Here, the signal and noise were measured at a fixed laser power of 400 mW. The signal from a stoichiometric mixture and the background noise increase with increasing PMT input voltage, but the signal-to-noise ratio initially increases until it reaches a maximum value of about 30 at 900 V after which decreases slightly. Therefore, a PMT input voltage of 900 V was chosen for the best signal-to-noise ratio.

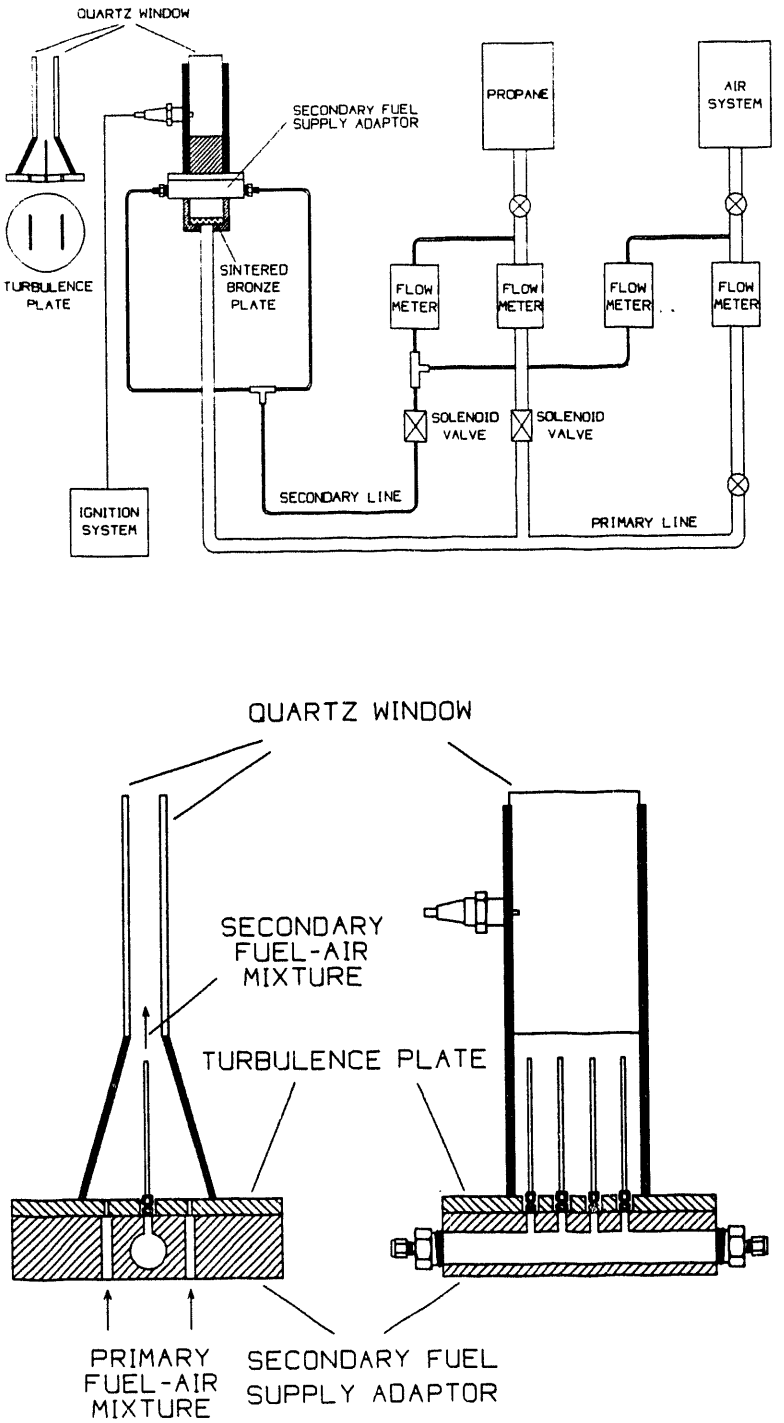

Figure 1. Turbulent flow system.

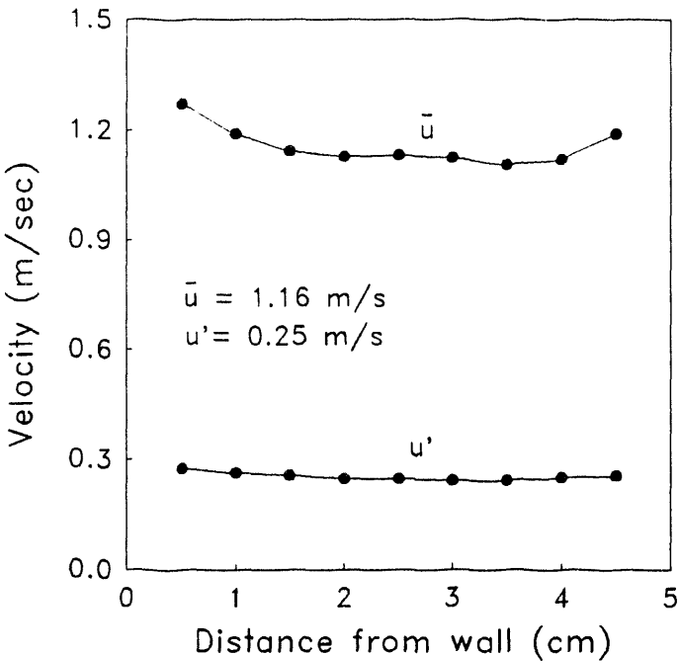

Figure 2. Mean velocity and turbulence intensity distribution in the test section.

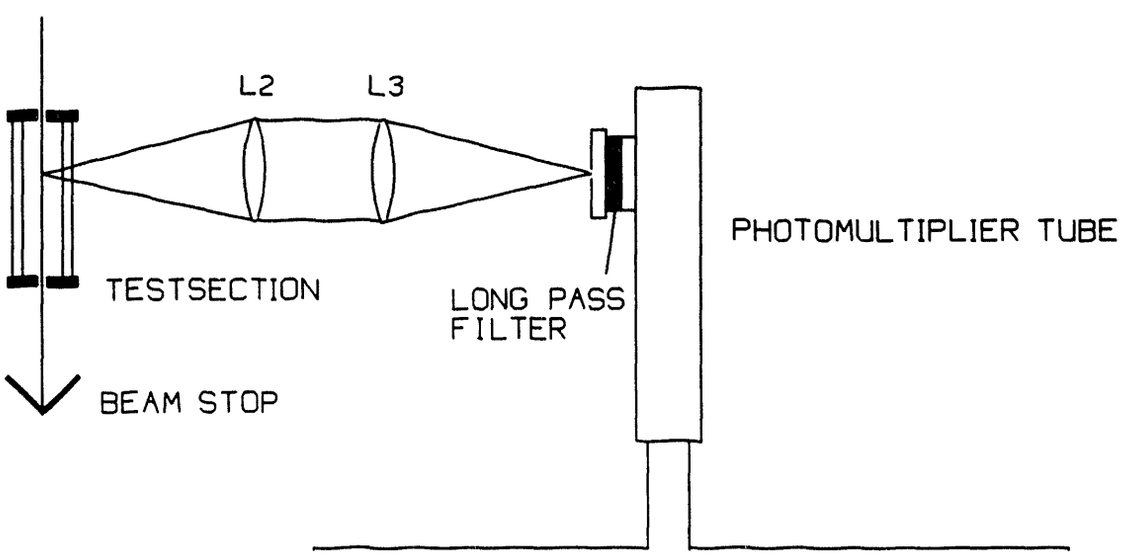

Figure 3. Schematic diagram of laser-induced fluorescence (LIF) technique.

The ensemble averaged mean and relative RMS fluctuation of the NO_2 fluorescence signal as functions of the fuel/air equivalence ratio under premixed conditions are shown in Fig. 4. The mean fluorescence signal increases linearly with the fuel/air equivalence ratio while the relative RMS fluctuation decreases. At stoichiometry ($\phi = 1.0$), the mean fluorescence signal is about 730 mV and the relative RMS fluctuation is about 5.2%. Because the premixed mixtures are homogeneous, there should be no significant fluctuation in the signal. However, the signal always includes small fluctuations due to fluctuations in laser power, room lights, and stray laser light. The RMS fluctuation does not increase as rapidly as the mean signal; therefore, the relative RMS fluctuation decreases with increasing fuel/air equivalence ratio. By using the linear relationship between the mean fluorescence signal and the fuel/air equivalence ratio, a transient fluorescence signal can be converted to a fuel/air equivalence ratio.

A fast data sampling rate was required to temporally resolve the fluctuations in the fuel/air equivalence ratio. The temporal resolution of this technique is primarily dependent on the device used to record the transient fluorescence signal. In this study, all transient fluorescence signals were recorded for 5 seconds at a sampling rate of 1 KHz, which was found to be adequate to resolve the temporal fluctuations. Five thousand data were recorded for each measurement, from which the ensemble averaged mean value and its RMS fluctuation were calculated. Figure 5 shows typical fuel/air equivalence ratio versus time traces for the premixed and four incompletely mixed cases, measured at the height of the spark electrode and at the center of the test section. As previously explained, the signal trace for the premixed case shows a little fluctuation due to measurement noise but this fluctuation is small compared to those of the incompletely mixed cases. The RMS fluctuations of the incompletely mixed cases are determined by assuming the measurement noise is uncorrelated with the fuel/air fluctuations, in which case the measured RMS fluctuation is equal to the square root of the sum of the square of the actual RMS fluctuation and the square of the noise RMS fluctuation. The relative RMS fluctuations calculated from the traces in Fig. 5 are 0%, 5%, 13%, 22% and 31% for the 100% premixed, 75% premixed, 50% premixed, 25% premixed and 0% premixed cases, respectively.

It is useful to know the characteristic size of the fuel/air "pockets" under incompletely mixed conditions. This can be estimated from the integral time scale, T, of the fuel/air fluctuations, which is defined by

$$T \equiv \int_0^\infty \rho(\tau)\, d\tau \tag{1}$$

where $\rho(\tau)$ is the autocorrelation coefficient which is given by

$$\rho(\tau) = \rho(-\tau) \equiv \frac{\overline{\phi'(t)\phi'(t')}}{\overline{\phi'^2}} \tag{2}$$

where $\overline{\phi'(t)\phi'(t')}$ is the correlation between values of the fluctuations in fuel/air equivalence ratio, $\phi'(t) = \phi(t) - \bar{\phi}(t)$, at times t and t'. In a turbulent flow, the value of T is a rough measure of the interval over which $\phi'(t)$ is correlated with itself. The integral length scale Λ, which can be interpreted as the characteristic size of the fuel/air "pockets", is then obtained by

$$\Lambda \equiv U\, T \tag{3}$$

where U is the mean flow velocity. This is called the Lagrangian integral length scale. On the other hand, the Eulerian integral length scale can be obtained by spatial correlations between two fixed points in a fixed frame of reference. These two length scales are the same if the turbulence is homogeneous and isotropic [34]. The autocorrelation coefficient curves corresponding to the fuel/air equivalence ratio traces in Fig. 5 are shown in Fig. 6. Also shown in this figure are the integrated areas under the autocorrelation curves which define the Lagrangian integral time scale. The integral length scale based on these measurements is estimated to be about 6 mm. This agrees well with the turbulent velocity field integral length scale of 4 mm, based on two-point spatial correlation measurements made in a nearly identical flow system [32].

Another useful way to characterize the incompletely mixed cases is in terms of the probability density functions (PDF's) of the fuel/air equivalence ratio which are shown in Fig. 7. These curves have a shape somewhat similar to the Gaussian distribution which is typical of probability densities measured in a turbulent flow, showing that fuel and air mixing is primarily controlled by the turbulent flow. As the degree of incomplete fuel-air mixing increases the peak value decreases and the curve becomes wider. The peak values are located close to $\phi = 1.0$, except for the 0% premixed case which is skewed a little to the lean side.

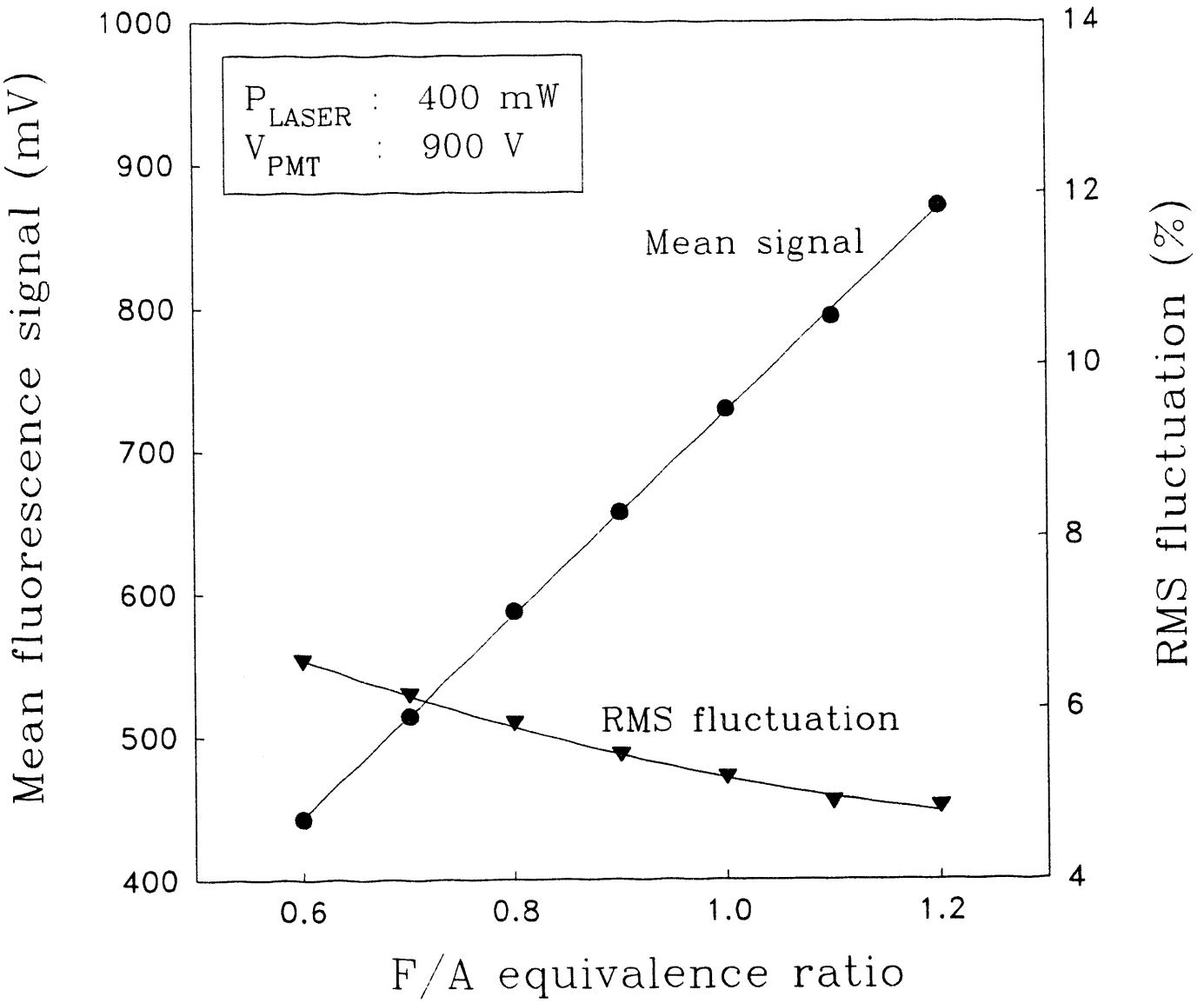

Figure 4. The mean and root-mean-square (RMS) fluctuation of NO_2 fluorescence signal as functions of the fuel/air equivalence ratio.

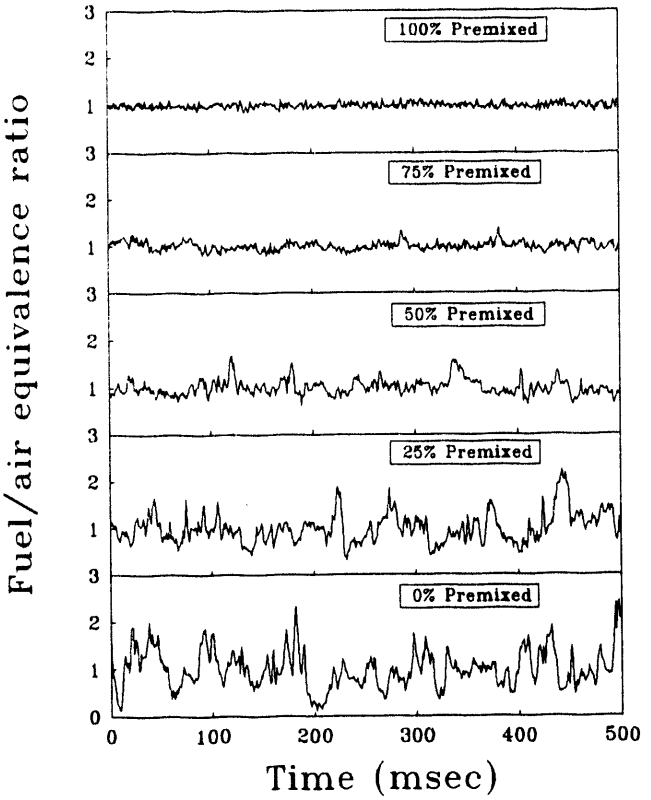

Figure 5. Typical fuel/air equivalence ratio vs. time traces for the premixed and four incompletely mixed cases.

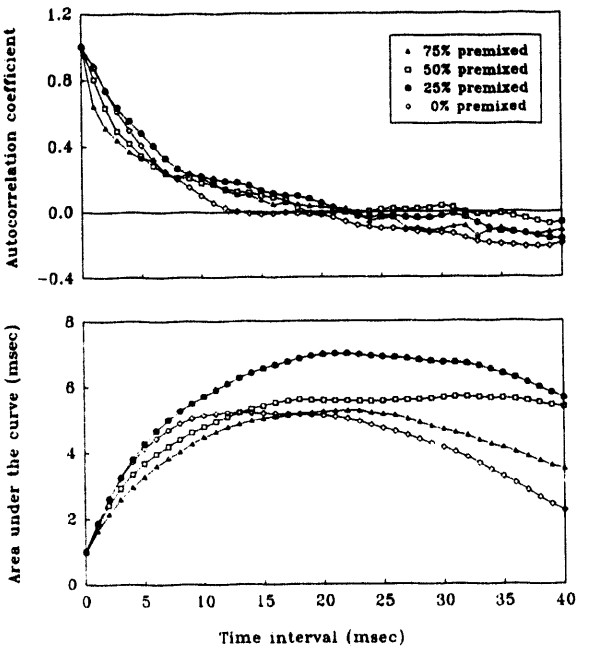

Figure 6. The autocorrelation coefficient curves corresponding to the fuel/air equivalence ratio traces in Fig. 5.

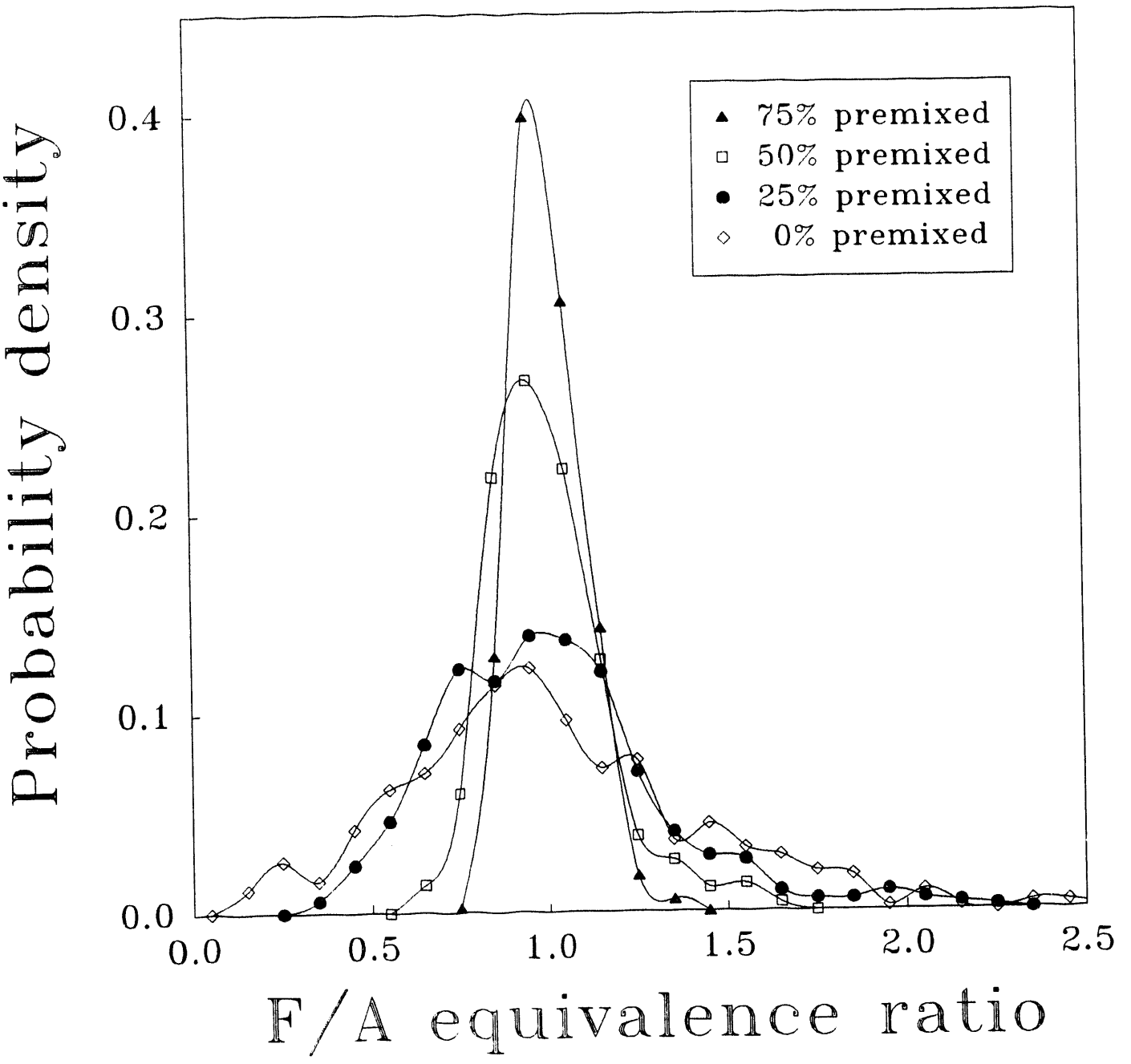

Figure 7. Probability density functions (PDF's) corresponding to the fuel/air equivalence ratio traces in Fig. 5.

The spatial distribution of mean fuel/air equivalence ratio and its RMS fluctuation across the test section is shown in Fig. 8. Measurements for each case were made over the width of the test section at nine locations which are at the height of the spark electrode and along the centerline of the test section. The mean and RMS fluctuation in fuel/air equivalence ratio is uniformly distributed across the test section. The mean fuel/air equivalence ratios averaged over the nine locations are, of course, 1.0 for all cases. The RMS fluctuations averaged over the nine locations are 0%, 6%, 13%, 24% and 33% as the degree of incomplete fuel-air mixing varies from the 100% premixed case to the 0% premixed case.

IGNITION SYSTEM - A General Motors High Energy Ignition (HEI) system was used as the ignition system for this study [35]. It consists of an ignition module, an ignition coil, a triggering circuit, a J-gap spark plug with 1.2 mm gap spacing (Champion Z-8), and a 12 VDC power supply. The ignition spark is initiated by a TTL pulse (5 V and 5 msec) provided by a pulse generator. Upon receiving the TTL pulse, the ignition module shorts out the primary side of the ignition coil, causing a high voltage rise on the secondary side. The high voltage induced in the secondary coil is routed to the spark plug to produce the ignition spark. A plot of measured spark power and energy delivered to the spark gap versus time is shown in Fig. 9. The HEI spark supplies total ignition energy of 60 mJ in about 4 msec spark duration, however ~ 80% of the energy is delivered in the first 2 msec. The variation in measured spark energy from spark to spark was less than 5%.

LASER SHADOWGRAPHY - High speed laser shadowgraphy was used to record the temporal evolution of the spark-ignited flame kernels. The experimental setup is illustrated in Fig. 10. A 514.5 nm-wavelength green beam from a continuous wave argon-ion laser was expanded by a spatial filter, and collimated by a concave mirror. The parallel, uniform intensity light was passed through the quartz windows in the test section , and then focused onto a camera by another concave mirror. The shadowgraph images were recorded using a high speed motion analysis system (Kodak Spin-Physics SP2000). Measurements were made at 4000 frames per second (fps) speed which corresponds to 250 μs between frames. At each operating condition, flame kernel images of twenty separate ignition events were recorded.

TEST CONDITIONS - Table 1 shows the test conditions used in this experiment. Stoichiometric propane-air mixtures with various degrees of incomplete fuel-air mixing were supplied to the test section at a flow rate corresponding to a nominal 1 m/sec mean flow velocity. The pressure and temperature were 1 atm and 300 K, respectively. The mean velocity and turbulence intensity were 1.16 m/sec and 0.25 m/sec, respectively. The integral length scale of the turbulent velocity fluctuations was estimated to be 4 mm [32]. The premixed and four incompletely mixed cases were established as test conditions. The relative RMS fluctuations in the fuel/air equivalence ratio are 0%, 6%, 13%, 24% and 33% for the 100% premixed, 75% premixed, 50% premixed, 25% premixed and 0% premixed cases, respectively.

ANALYSIS METHOD - The flame kernel images recorded on the SP2000 system were transferred to a VHS tape. The images on the VHS tape were projected onto a screen using a VCR and a front-projection TV. The flame kernel boundary was digitized by manually tracing the flame kernel boundary, and the coordinates were stored in a computer. Based on the X-Y coordinates of the flame kernel boundary and a scale factor, the projected area enclosed by the flame kernel boundary was determined. An equivalent flame kernel radius was defined as that of a semi-circle whose area was the same as the projected area of the flame kernel. This digitizing process was repeated for 20 separate ignition events at each operating condition, producing twenty individual equivalent radius-versus-time curves. These twenty cases were used to calculate an average equivalent radius and its standard deviation. The average growth rate was obtained by taking the derivative of the average equivalent radius-versus-time curve.

The average growth rate was compared with the laminar growth rate of the flame kernel at each test condition. Based on continuity, the laminar growth rate is defined as

$$\left[\frac{dr}{dt}\right]_{lam} = \frac{\rho_u}{\rho_b} S_L \tag{4}$$

where ρ_u and ρ_b are unburned and burned gas density, respectively, and S_L is the laminar flame speed. The burned gas density was calculated using the NASA equilibrium code [36]. The unburned gas density was determined from the ideal gas law. The laminar flame speed for propane-air mixtures as a function of the diluent mass fraction was

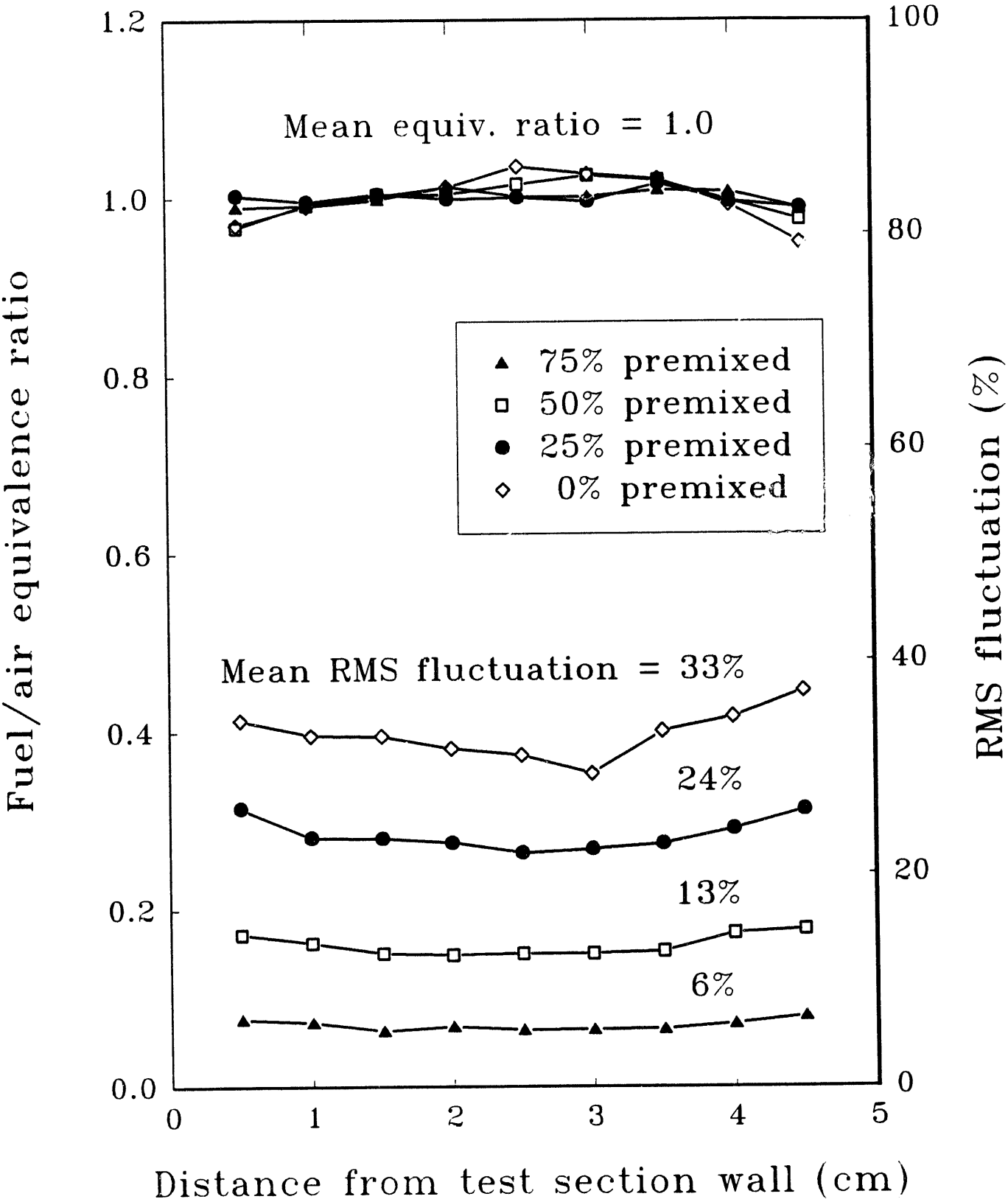

Figure 8. The distribution of mean fuel/air equivalence ratio and its RMS fluctuation in the test section.

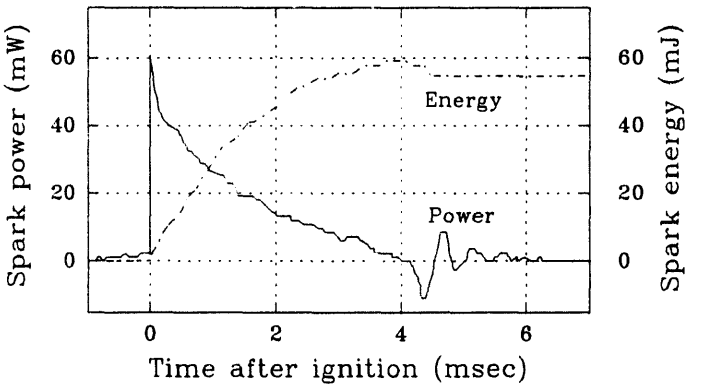

Figure 9. Power and energy delivered to spark gap versus time after the start of ignition.

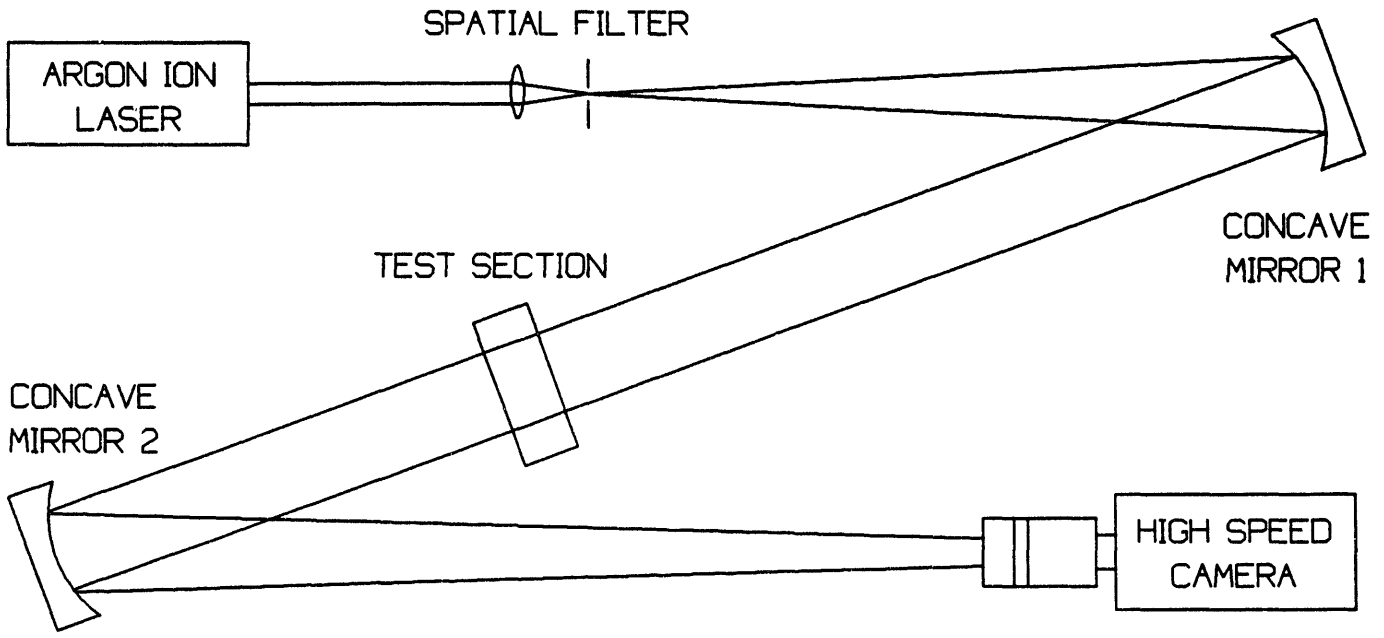

Figure 10. Schematic diagram of laser shadowgraphy technique.

Table 1. Test Conditions

Fuel	Propane
Pressure	1 atm
Temperature	300 K
Flow characteristics	
Mean velocity	1.16 m/sec
Turbulence intensity	0.25 m/sec
Relative turbulence intensity	22 %
Integral length scale	~ 4 mm
Fuel-air mixedness	**RMS fluctuation**
100% premixed case	0%
75% premixed case	6%
50% premixed case	13%
25% premixed case	24%
0% premixed case	33%

obtained from

$$S_L = (1 - 3.0f)\, S_L(0) \tag{5}$$

where $S_L(0)$ is the unstretched, adiabatic laminar flame speed without dilution and f is the diluent mass fraction [37-39]. The unstretched, adiabatic laminar flame speed (in cm/sec) for propane-air mixtures without dilution as a function of fuel/air equivalence ratio at a temperature of 298 K and pressure of 1 atm is given by

$$S_L(0) = 38.31 + 24.84(\phi - 1) - 153(\phi - 1)^2 \tag{6}$$

where ϕ denotes the fuel/air equivalence ratio [40].

RESULTS AND DISCUSSION

Incomplete fuel-air mixing affects early flame kernel growth due to spatial and temporal variations in the local mixture strength near the spark plug which result in ignition-to-ignition variations in the flame kernel growth rate. This is especially true for the early stages of flame kernel development when the flame is small and not highly wrinkled, and flame kernel growth is primarily dependent on the laminar burning velocity. Variations in the local equivalence ratio, such as shown in Fig. 7, not only affect the laminar flame speed but also thermal expansion due to a change in the flame temperature. Flame stretch and preferential diffusion also have a significant impact on flame kernel growth. The primary effect of flame stretch and preferential diffusion is a change in the laminar burning velocity resulting from a change in the flame temperature. For rich propane-air mixtures where the effective Lewis number is less than unity, the flame temperature and flame speed increase with increasing flame stretch because the fuel/air equivalence ratio shifts closer to stoichiometric at the flame front. The reverse is true for lean propane-air mixtures where the effective Lewis number is greater than unity [41]. In 1969, Palm-Leis and Strehlow [42,43] investigated the effect of flame stretch on the burning velocity of an outwardly propagating spherical flame in laminar and isotropic turbulent flow fields. In the laminar case, rich propane-air mixtures exhibited a higher burning velocity at small radii, while lean mixtures showed a lower burning velocity at small radii. Their results indicate that the effect of preferential diffusion on laminar burning velocity is very high during the early stages of flame kernel development and that it changes its sign as the fuel/air equivalence ratio passes through unity. However, this effect diminishes rapidly as the flame kernel grows in size, and becomes negligible as the flame kernel radius approaches 20 - 30 mm. Based on the above considerations, the results from this study are presented and discussed below.

The shadowgraph images of the flame kernels show in all cases that the flame kernel grows outward from the spark electrode in a somewhat semi-circular shape, but with a noticeable stretching of the flame kernel in the direction of the gas flow. Note, however, that the convection of the flame kernel does not cause it to separate from

the electrodes at any of the test conditions. As the degree of incomplete fuel-air mixing increases, more wrinkles are observed on the flame kernel surface. Note that the fuel and air mix as the mixture flows through the test section, therefore the wrinkles develop mostly on the upstream part of the flame kernel surface. The effect of incomplete fuel-air mixing on the "cyclic" variation of flame kernel growth is shown in Fig. 11, where twenty individual growth curves for each test condition are plotted versus time after the start of ignition. Only successful ignition cases, i.e., no misfire cases, are included in these results. The size of the flame kernel after the blast wave phase, called the initial flame kernel size below, can be estimated from these measurements by extrapolating the flame kernel radius versus time curves back to t = 0. Since only one ignition system was used, the ignition system parameters were fixed so that the initial flame kernel radius is ~2.5 mm (~5 mm diameter) for all cases. Comparing this to the characteristic size of the fuel/air pockets, which was previously determined to be approximately 6 mm, indicates that even the initial flame kernel is likely to encounter variations in the fuel/air equivalence ratio over its surface in the incompletely mixed cases.

As shown in Fig. 11, the "cyclic" variations are smallest for the premixed case and appear to increase as the RMS fluctuation in the fuel/air equivalence ratio increases, where in particular more slow growth events are observed as the degree of incomplete mixing increases. These slow growth events may cause partial burn cycles in an SI engine which will increase the unburned hydrocarbon emissions and reduce the performance of the engine. Some faster events are also observed in the incompletely mixed cases because the laminar burning velocity of propane-air mixtures peaks at slightly fuel rich conditions [37,44].

The observed variations in the flame kernel size at later times are generally believed to be the result of the fluctuations in the early flame kernel growth rate. To quantify the effect of the early flame kernel growth rate on the subsequent flame kernel size, the empirical coefficient of correlation $R(t_1,t_2)$ was calculated as in Eq. 7.

$$R(t_1,t_2) = \frac{\frac{1}{N}\sum_{i=1}^{N} \frac{dr_i'}{dt}(t_1)\, r_i'(t_2)}{\left[\left[\frac{dr_i'}{dt}(t_1)\right]^2 \overline{[r_i'(t_2)]^2}\right]^{\frac{1}{2}}} \qquad (7)$$

where

N = number of ignition events

$\frac{dr_i'}{dt}(t) = \frac{dr_i}{dt}(t) - \overline{\frac{dr}{dt}(t)}$

$r_i'(t) = r_i(t) - \overline{r(t)}$

t = time after the start of ignition (msec)

$\frac{dr_i}{dt}(t)$ = i-th flame kernel growth rate at time t

$r_i(t)$ = i-th flame kernel radius at time t.

The effect of the early growth rate on the flame kernel size at later times is shown in Fig. 12, where the correlation coefficients are expressed as functions of t_1 with a fixed t_2 of 6 msec. Thus the correlation coefficient curves show how well the growth rate at t_1 correlates with the flame kernel size at 6 msec (6 msec corresponds to 36 crankangle degrees at 1000 rpm). Note that all curves have two distinctive regions; the first region up to 2 msec and the second region at 2-4 msec. In the first region the correlation coefficients are initially small and increase with increasing time. The most likely explanation for this is that the early growth rate, i.e. before 2 msec, is strongly influenced by spark assisted growth since it is during this time that the spark deposits approximately 80% of its energy. The reason why this results in a poor correlation is that the spark assisted growth rate is not strongly affected by the local equivalence ratio or turbulent flow conditions (at this relatively low mean velocity and turbulence intensity); where as the later growth rate (i.e. from 2-4 msec) is strongly dependent on both the local equivalence ratio and turbulence conditions. This is also evident from close inspection of the flame kernel growth data shown in Fig. 11. These observations are consistent with flame kernel growth and cylinder pressure correlation fig. 11

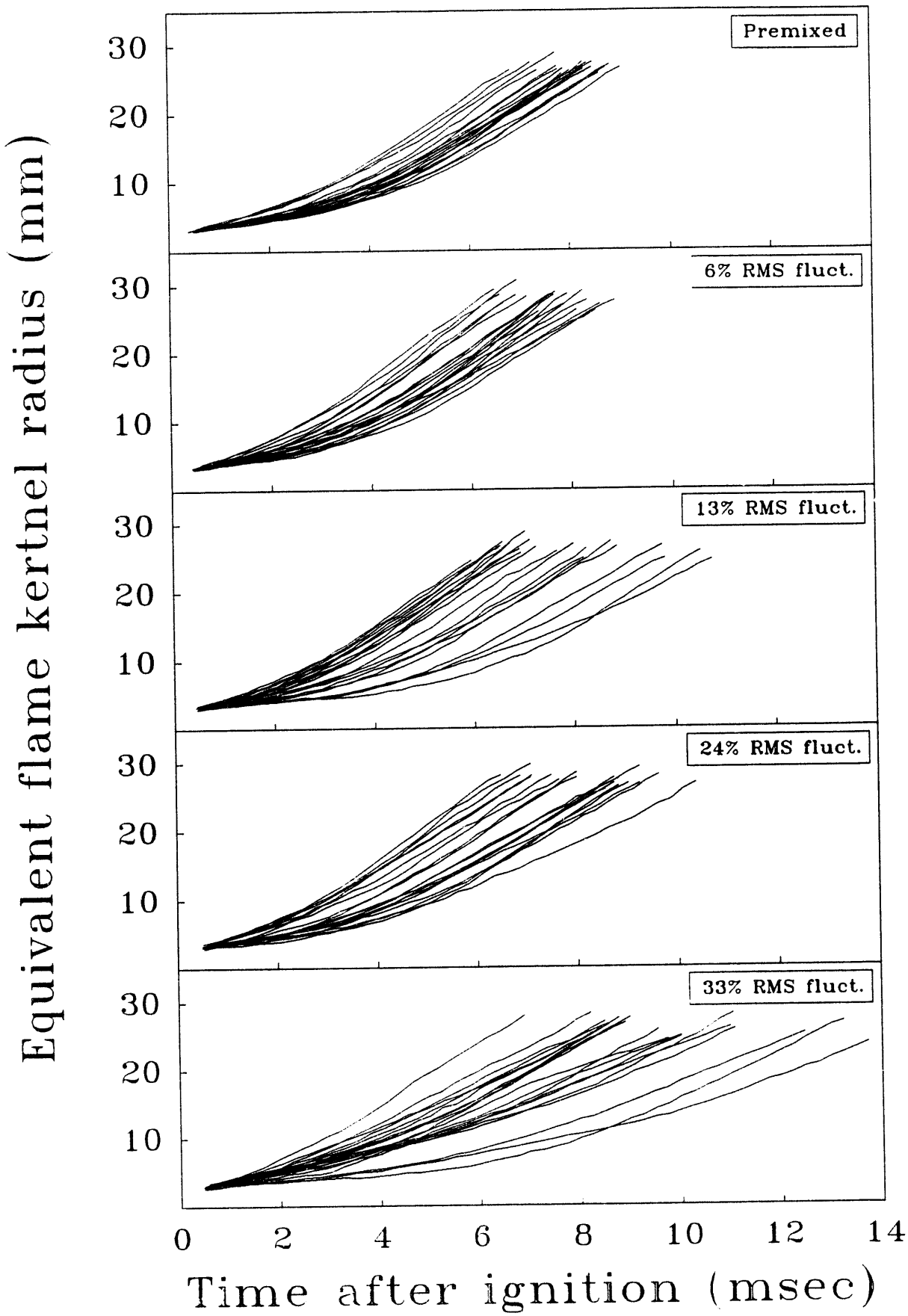

Figure 11. Twenty individual growth curves for each test conditions showing "cyclic" variation in the flame kernel growth.

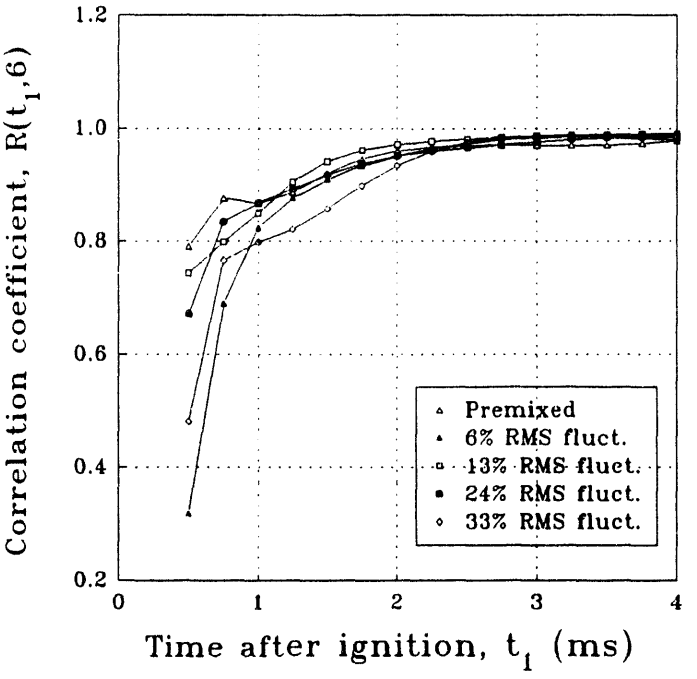

Figure 12. Correlation coefficient $R(t_1, 6)$ as a function of t_1 with a fixed t_2 of 6 msec.

measurements made in an optically accessible engine operating with the same ignition system [45]. Similarly they are consistent with the relatively poor correlation between optical fiber spark plug measurements and cylinder pressure measurements [46]. Note, however, that in a situation with high mean velocity and high turbulence intensity, the local velocity fluctuations could affect the spark, resulting in a stronger correlation between the spark assisted growth and the subsequent flame kernel size.

The correlation between the early growth rate and the subsequent size of the flame kernel, however, becomes more significant as t_1 approaches 2 msec where the second region begins, indicating that by this time there are significant "cyclic" variations in the growth rate which directly result in variations in the subsequent size of the flame kernel. In the second region, the growth rate correlates well with the flame kernel size at 6 msec, and the curves are virtually flat with correlation coefficients of 0.96 or higher.

And finally, note that incomplete fuel-air mixing appears to result in poorer correlations during the spark assisted growth phase (0-2 msec), but does not significantly affect the correlation during the later stages (2-4 msec).

The effect of incomplete fuel-air mixing on the mean flame kernel growth is shown in Fig. 13, where the mean flame kernel radius is plotted versus time after the start of ignition. The mean growth curves were obtained by averaging twenty ignition events for each case in Fig. 11. The mean growth of the flame kernel is a little faster in the 6%, 13% and 24%-RMS-fluctuation cases and a little slower in the 33%-RMS-fluctuation case than in the premixed case.

Before discussing these results it is important to determine whether or not the observed differences are significant given the relatively small sample size of 20. The 95% confidence interval for the mean μ is defined as where

$$CONF\{\bar{r}-k \le \mu \le \bar{r}+k\} \quad (8)$$

$\bar{r}$ = the mean of the sample

$k = 1.96\sigma/\sqrt{N}$

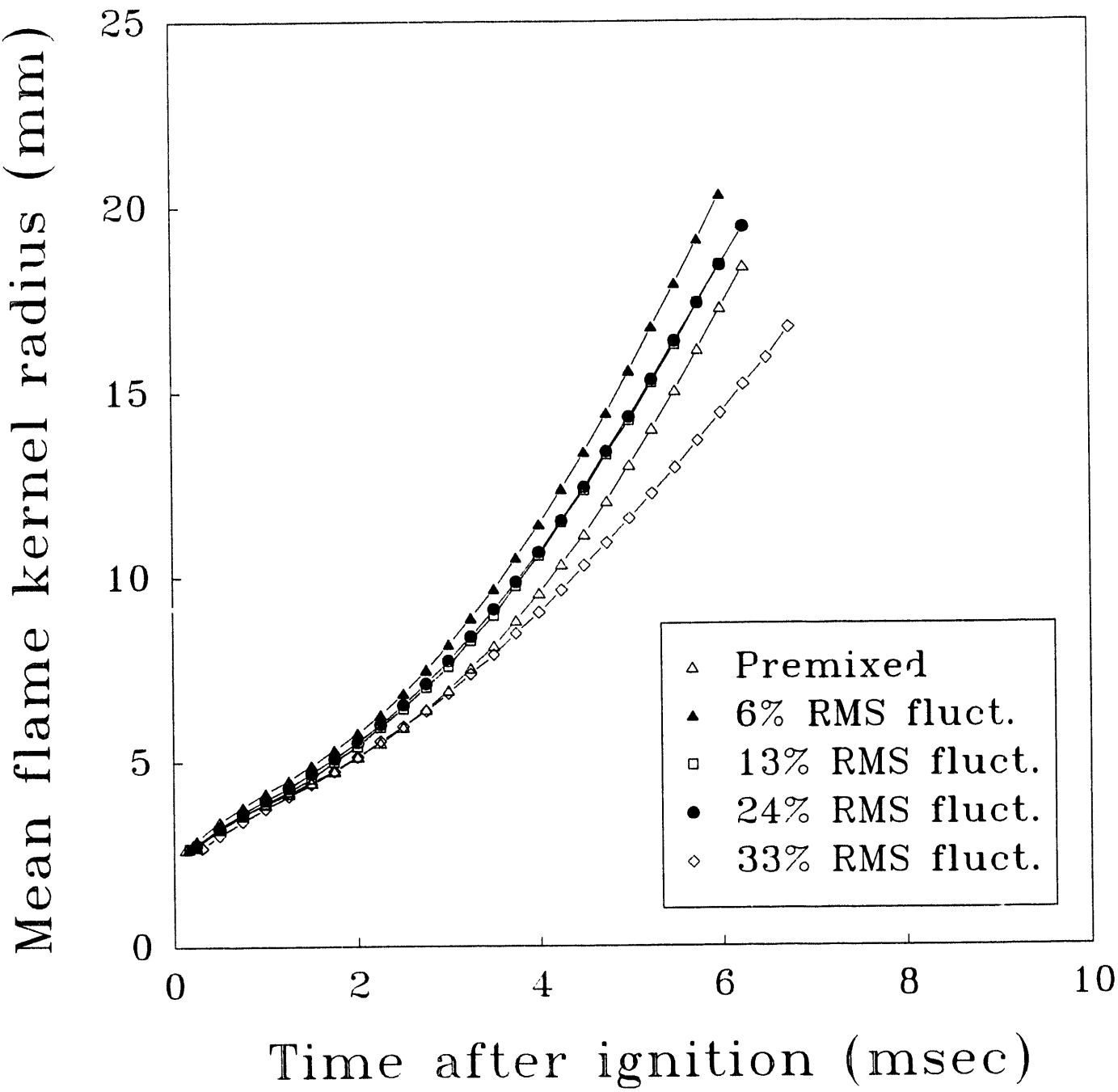

Figure 13. The mean growth curves versus time after ignition start.

Figure 14 shows the 95% confidence interval for the mean in the premixed, 6%-RMS-fluctuation and 33%-RMS-fluctuation cases. As shown, the statistical uncertainty in the mean flame kernel radius measurement is comparable to the differences between the different cases, therefore the discussion of the results which follows, while considered to be valid must be viewed with this in mind.

One factor affecting the flame kernel growth rate in the incompletely mixed cases is the variation in the laminar flame speed with fuel/air equivalence ratio [44]. This effect can be estimated using the fuel/air equivalence ratio PDF's shown in Fig. 7, where it is necessary to discard cases which fall outside the lean and rich flammability limits, i.e. $0.52 \leq \phi \leq 2.4$ for propane-air [47], in order to account for the fact that misfires are not included in the growth rate data. Table 2 gives the mean laminar flame speed, within the flammability limits, for the five test conditions, where it is seen that the mean laminar flame speed decreases with increasing RMS fluctuations in the fuel/air equivalence ratio. This means that the mean growth of the flame kernel should be slower in the incompletely mixed cases than in the premixed case, which does not agree with the experimental results, nor with the results reported in some studies which show that some form of heterogeneous intake charge is beneficial for engine operation [19,21].

Two other factors which must be considered under incompletely mixed conditions are the effects of flame stretch and preferential diffusion and the effect of flame front wrinkling. As discussed previously, the early flame kernel experiences significant flame stretch which under fuel rich conditions results in an increase in the laminar flame speed and under fuel lean conditions results in a decrease in the laminar flame speed. Assuming a nearly symmetric fuel/air equivalence ratio PDF, this should have little effect in the mean flame kernel growth rate. The second factor to consider is the observed wrinkling of the flame kernel surface which has been found to increase with increasing RMS fluctuation in the fuel/air equivalence ratio. This fact will result in an increased flame surface area, which alone would contribute to an increased mean flame kernel growth rate.

Table 2. Mean laminar flame speed ($\overline{S_L}$) within flammability limits

	$\overline{S_L}$ (cm/sec)
Premixed	44
6%-RMS-fluctuation	42
13%-RMS-fluctuation	39
21%-RMS-fluctuation	33
33%-RMS-fluctuation	31

Figure 15 shows the mean growth rate of the flame kernel as a function of the mean flame kernel radius. For comparison, the previously defined laminar growth rate is also shown. The growth rate is initially very large, in fact, many times larger than the laminar growth rate [3]. The large initial growth rate is not shown in Fig. 15 because a recording speed of 4000 fps is not fast enough to resolve the initial growth rate. The result shows that this initial, large growth rate decreases very rapidly to a value which is less than the laminar growth rate, after which it increases to a value slightly greater than the laminar growth rate. This behavior can be explained in terms of three competing processes [3]. One is the effect of the thermo-chemical energy of the flame kernel which one would expect to be largest initially and to decrease with time. The second is the combined effect of flame stretch and preferential diffusion, which results in either a reduced or enhanced laminar flame speed depending on the fuel/air equivalence ratio, where this effect also decreases in magnitude as the flame kernel radius increases, such that by a radius of 20 to 30 mm it is nearly negligible [42,43]. The third effect is due to turbulence, which increases with time as the flame kernel grows until reaching a fully-developed state. One interesting behavior of the growth rate curves is that regardless of the different degree of incomplete fuel-air mixing, the mean growth rates reach a minimum and start to increase when the mean flame kernel radii are about 4 mm which corresponds to the integral length scale. This result shows that after the flame kernel grows to a size bigger than twice the integral length scale, turbulence effects enhance the growth rate by wrinkling and distorting the flame kernel surface.

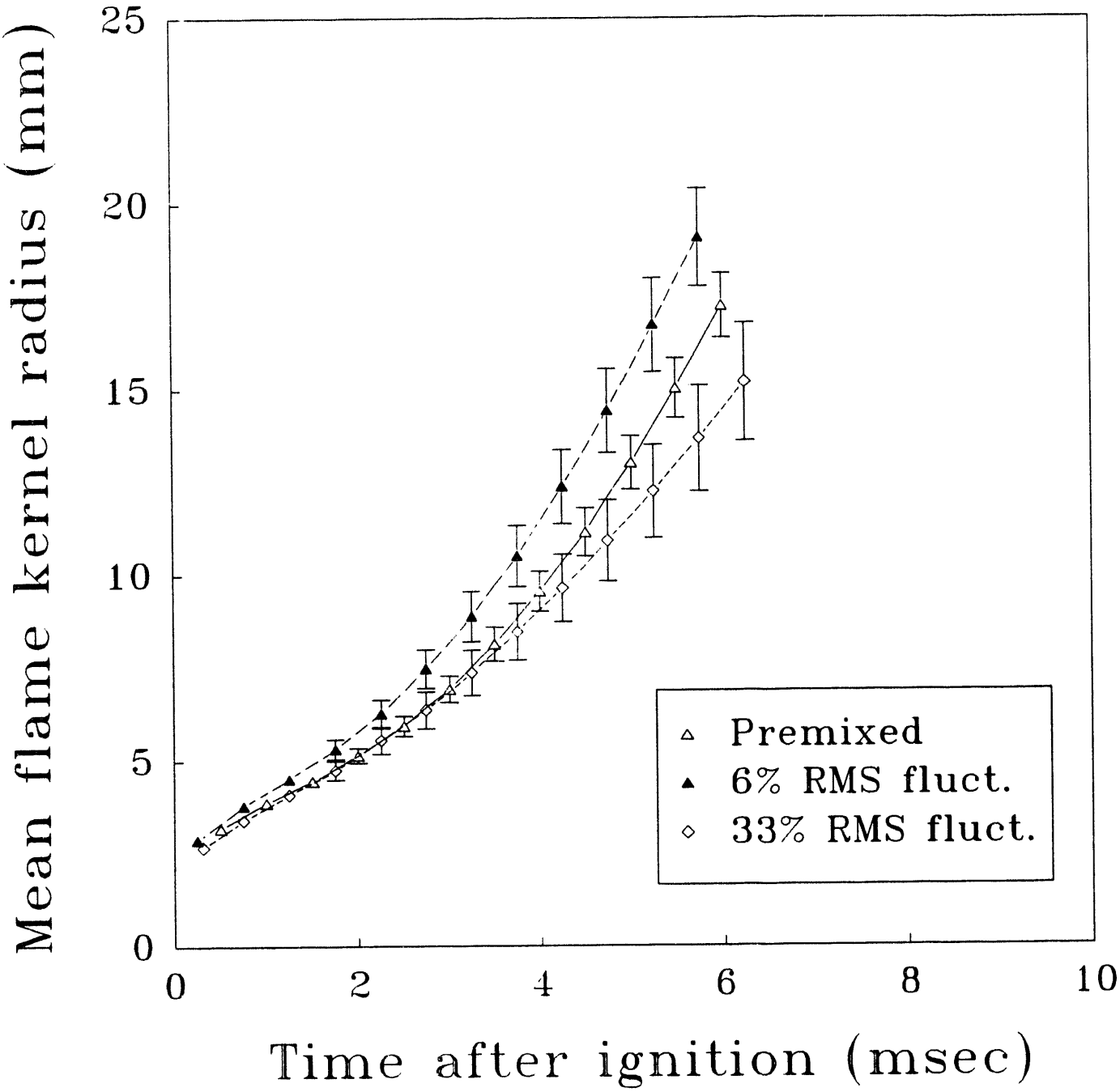

Figure 14. The 95% confidence interval for the mean in the premixed, 6%-RMS-fluctuation and 33%-RMS-fluctuation cases.

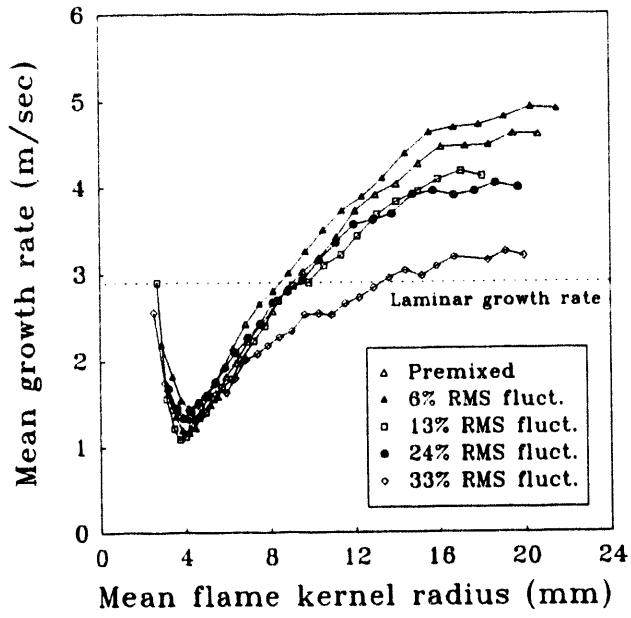

Figure 15. Mean growth rate of the flame kernel as a function of mean flame kernel radius.

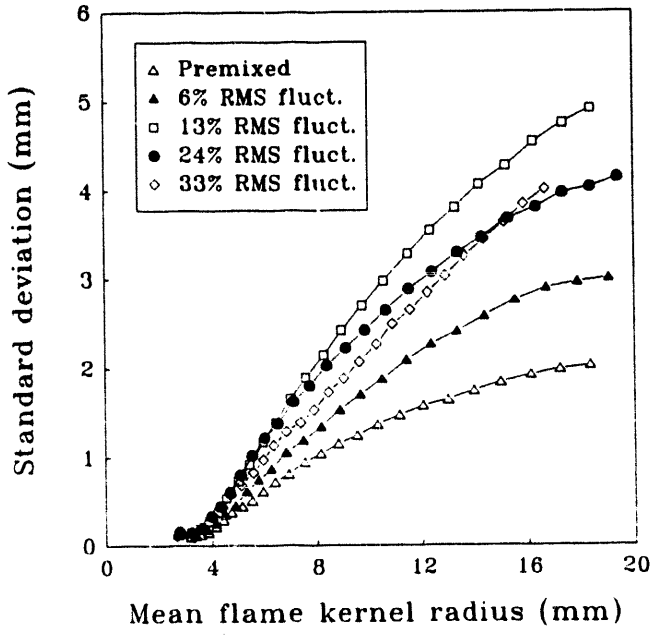

Figure 16. Standard deviation in flame kernel size versus mean flame kernel radius.

Similarly to the mean flame kernel growth, the mean growth rate for the 6%-RMS-fluctuation case is a little higher than for the premixed case as shown in Fig. 15. However, the growth rates for the premixed, 6%-RMS-fluctuation, 13%-RMS-fluctuation and 24%-RMS-fluctuation cases are not much different. Based on the discussions about the uncertainty of the experiments, one can say that the mean growth rates for these four cases are within the experimental error. However, the growth rate for the 33%-RMS-fluctuation case is significantly lower than those of the others, suggesting that large fluctuations in the fuel/air equivalence ratio may result in a low mean flame kernel growth rate. Therefore one may expect that with a higher degree of incomplete fuel-air mixing the application of lean-burn technology may be limited by partial burns.

Figure 16 shows the standard deviation in flame kernel size, which is a measure of the "cyclic" variation in flame kernel growth, versus mean flame kernel radius. As the flame kernel grows from its initial size (radius) of $\sim$2.5 mm to $\sim$4 mm the standard deviation is small and relatively constant. This corresponds to the time when flame kernel growth is primarily the result of spark assisted growth, as disscussed previously. After this time, however, flame kernel growth is strongly affected by the local fuel/air equivalence ratio and turbulence conditions and therefore begins to experience significant "cyclic" variations, as indicated by a marked increase in the standard deviation of the flame kernel radius. And finally, when the flame kernel radius reaches $\sim$20 mm, the standard deviation appears to begin to level off, suggesting that the size of the flame kernel is much larger than the scale of the fuel/air and turbulence fluctuations (which are $\sim$6 mm and $\sim$4 mm, respectively). Comparing the results for different RMS fluctuations in the fuel/air equivalence ratio it is clearly evident that incomplete fuel-air mixing can contribute significantly to "cyclic" variations in flame kernel growth, however, because of the limited statistical certainty of the measurements the relationship between the degree of incomplete mixing and the "cyclic" variations can not be accurately quantified.

It is well known that the fluid motion within the cylinder of an internal combustion engine has a major influence on the performance of the engine. The general motion within the cylinder and the associated turbulence, particularly during ignition and flame propagation, affects the mass burning rate, cycle-to-cycle variations, and the lean combustion limit [18,48-53]. An increase in turbulence initially improves engine efficiency due to more rapid combustion. Further increases in turbulence are progressively less beneficial and can ultimately lead to flame quenching, particularly in the case of lean mixtures. Incomplete fuel-air mixing can affect flame quenching through fluctuations in the fuel/air equivalence ratio. Flame quenching is most likely in the early phase of flame development, when the temperature and laminar flame speed are relatively low. This is particularly true for lean mixtures with low laminar flame speeds and high turbulence engines at high speeds since these conditions can lead to high values of the flame stretch rate, and affect the misfire limit.

The misfire tendency at various degrees of incomplete fuel-air mixing is shown in Fig. 17, where the misfire rate was determined by counting the number of misfire events in 100 ignition attempts. Misfire corresponds to a case when the flame kernel grows little if any beyond its initial size after which it is extinguished. This was observed with the high speed shadowgraph system and was found to coincide with the absence of a flame in the turbulence generating section upstream of the test section following ignition; therefore, this simple observation was used to determine whether a misfire occurred. The premixed and 6%-RMS-fluctuation cases had a 0% misfire rate. The misfire rates were 1% and 2% for the 13% and 24%-RMS-fluctuation cases, respectively; however, it rapidly increased to 23% in the 33%-RMS-fluctuation case.

It may be useful to compare the misfire rates with the fraction of fuel/air equivalence ratios beyond the flammability limits, which can be obtained from the PDF curve for each case shown in Fig. 7. There are no non-flammable fuel/air equivalence ratios for the premixed, 6% and 13%-RMS-fluctuation cases. By increasing the degree of incomplete fuel/air mixing, these are increased to 3% of the total PDF in the 24%-RMS-fluctuation case and 10% of the total PDF in the 33%-RMS-fluctuation case. The percentage of non-flammable fuel/air equivalence ratios, however, does not completely explain the observed misfire rates for the 13%, 24% and 33%-RMS-fluctuation cases. This is to be expected, though, since successful ignition and flammability are not the same, e.g. ignition is a transient phenomenon and flammability is a steady state phenomenon. Successful ignition is also dependent on the details of the ignition system. Another approach would be to select the lean misfire limit fuel/air equivalence ratio which gives the correct misfire rate for the 13%-RMS-fluctuation case and apply it to the other cases. If one does this one

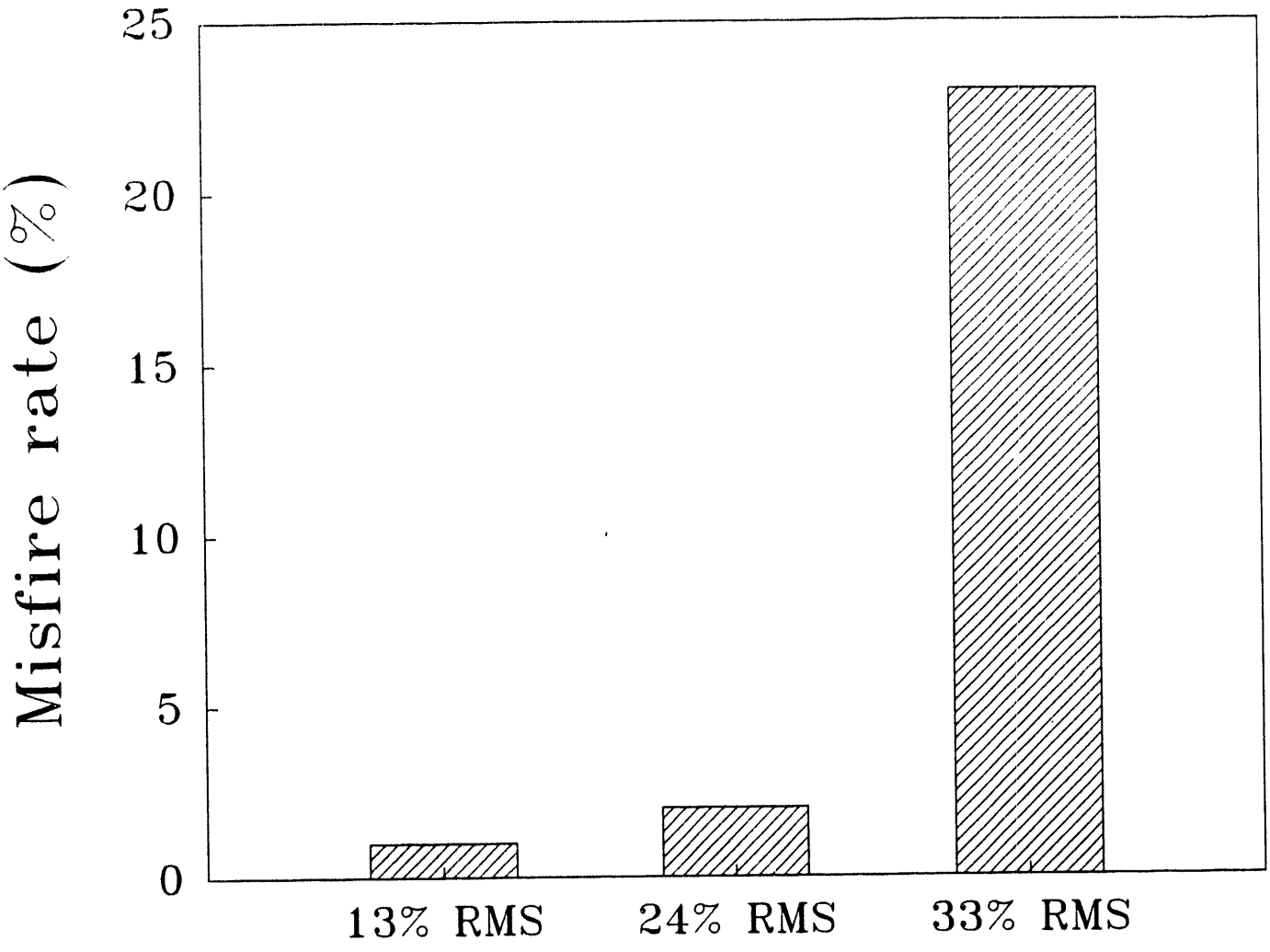

Figure 17. The misfire tendency at various degrees of incomplete fuel-air mixing.

finds that the lean misfire limit fuel/air equivalence ratio is 0.6 which when applied to the fuel/air equivalence ratio PDF's for the 6%, 24% and 33%-RMS-fluctuation cases predicts misfire rates of 0%, 8%, and 16%, respectively. These, however, still do not agree with the actual mixfire rates.

CONCLUSIONS

The effect of incomplete fuel-air mixing on spark-ignited flame kernel growth has been studied in terms of its effect on the flame kernel growth rate, the "cyclic" variation in the flame kernel growth and the misfire rate. The experiments were conducted at 1 atm, 300 K conditions in a turbulent flow system which allows for independent variation of flow field parameters and the degree of fuel-air mixing. The mean velocity and turbulence intensity were fixed at 1.16 and 0.25 m/sec, respectively. Five cases were studied; a premixed and four incompletely mixed cases with 6%, 13%, 24% and 33% RMS fluctuations in the fuel/air equivalence ratio. The overall fuel/air equivalence ratio was unity for all cases. The main conclusions from this study are summarized below (Here, the quantitative results should be used with caution, however, due to the statistical uncertainty of the measurements):

1. The initial size of the flame kernel was not affected by the degree of incomplete fuel-air mixing.

2. The fluctuation in local mixture strength due to incomplete fuel-air mixing causes wrinkling and distortion of the flame kernel surface. As the RMS fluctuation in the fuel/air equivalence ratio increases, more wrinkles on the flame kernel surface can be found.

3. The "cyclic" variations in flame kernel growth for the incompletely mixed cases are greater than for the premixed case.

4. A strong correlation ($R(t_1,6) > 0.9$) between the early flame kernel growth rate and the subsequent size of the flame kernel was not achieved until after ~ 2 msec, i.e. until the completion of the spark assisted growth phase.

5. The mean growth of the flame kernel is within the experimental uncertainty for all test conditions except the 33%-RMS-fluctuation case which is significantly slower.

6. The standard deviation in flame kernel size, which is a measure of the "cyclic" variation in flame kernel growth, is small and relatively constant during the spark assisted growth phase (0-2 msec), after which it increases markedly until the flame kernel radius is ~20 mm. The standard deviations for the incompletely mixed cases are higher than in the premixed case, but no consistent trend was found.

7. The premixed and 6%-RMS-fluctuation cases had a 0% misfire rate. The misfire rates were 1% and 2% for the 13% and 24%-RMS-fluctuation cases, respectively; however, it rapidly increased to 23% in the 33%-RMS-fluctuation case.

REFERENCES

1. Amann, C. A., "Whither the Spark-Ignition engine?," GMR-4598, 1984.
2. Heywood, J. B., Internal Combustion Engine Fundamentals, McGraw-Hill, 1988.
3. Cho, Y. S., Santavicca, D. A. and Sonntag, R. M., "The effect of Spark Power on Spark-Ignited Flame Kernel Growth," SAE Paper 922168, 1992.
4. Nakamura, N., Kobayashi, T., Hanaoka, M., and Takagi, N., "A New Platinum Tipped Spark Plug Extends the Lean Misfire Limit," SAE Paper 830479, 1983.
5. Pischinger, S. and Heywood, J. B., "How Heat Losses to the Spark Plug Electrodes Affect Flame Kernel Development in an SI-Engine," SAE Paper 900021, 1990.
6. Tanuma, T., et al., "Ignition Combustion, and Exhaust Emissions of Lean Mixtures in Automotive Spark Ignition Engines," SAE Paper 710159, 1971.
7. Anderson, R. W. and Asik, J. R., "Ignitability Experiments in a Fast Burn, Lean Burn Engine," SAE Paper 830477, 1983.
8. Anderson, R. W. and Asik, J. R., "Lean Air-Fuel Ignition System Comparison in a Fast-Burn Engine," SAE Paper 850076, 1985.
9. Pischinger, S. and Heywood, J. B., "A Study of Flame Development and Engine Performance with Breakdown Ignition Systems in a Visualization Engine," SAE Paper 880518, 1988.
10. Anderson, R. W., "The Effect of Ignition System Power on Fast Burn Engine Combustion," SAE Paper 870549, 1987.
11. Asik, J. R., et al., "Design of a Plasma Jet Ignition System for Automotive Application," SAE Paper 770355, 1977.
12. Nakai, M., Nakagawa, Y., Hamai, K., and Sone, M., "Stabilized Combustion in a Spark-Ignited Engine through a Long Spark Duration," SAE Paper 850075, 1985.
13. Harrington, J. A., Shinsu, R. C., and Asik, J. R., "A Study of Ignition System Effects on Power, Emissions, Lean Misfire Limit, and EGR Tolerance of a Single-Cylinder Engine - Multiple Spark versus Conventional Single Spark Ignition," SAE Paper 740188, 1974.
14. Kono, M., et al., "Spark Discharge Characteristics and Igniting Ability of Capacitor Discharge Ignition Systems," Combust. Sci. and Tech., Vol. 19, pp. 13-18, 1978.
15. Maly, R,. Et al., "Prospects of Ignition Enhancement," SAE Paper 830478, 1983.

16. Maly, R., "Spark Ignition: Its Physics and Effect on the Internal Combustion Engine," in: Fuel Economy: Road Vehicles Powered by Spark Ignition Engines, Eds., J. C. Hillard, and G. S. Springer, Chapter III, Plenum Press, 1984.
17. Ziegler, G. F. W., et al., "Influence of a Breakdown Ignition System on Performance and Emission Characteristics," SAE Paper 840992, 1984.
18. Ho, C. M., and Santavicca, D. A., "Turbulence Effects in Early Flame Kernel Growth," SAE Paper 872100, 1987.
19. Peters, B. D. and Quader, A. A., ""Wetting" the Appetite of Spark Ignition Engines for Lean Combustion," SAE Paper 780234, 1978.
20. Pundir, B. P., Zvonow, V. A., and Gupta, C. P., "Effect of Charge Non-Homogeneity on Cycle-by-Cycle Variations in Combustion in SI Engines," SAE Paper 810774, 1981.
21. Kajitani, S., Sawa, N., and Rhee, K. T., "Mixture Preparation in Spark-Ignition Engine and its Effect on Engine Performance and Combustion Characteristics," SAE Paper 900711, 1990.
22. Sztenderowicz, M. L., and Heywood, J. B., "Mixture Nonuniformity Effects in S.I. Engine Combustion Variability," SAE Paper 902142, 1990.
23. Daniels, C. H., Evers, L. W., and Han Z., "Evaluating the Influence of Fuel Preparation on the Performance of a Spark-Ignited Engine," ICLASS-91, July 1991.
24. Gulati, A., and Warren, R. E., Jr., "NO_2-Based Laser-Induced Fluorescence (LIF) Technique to Measure Cold-Flow Mixing," AIAA 30th Aerospace Sciences Meeting & Exhibit, Jan. 1992.
25. Kadota, T., "The Application of Laser Rayleigh Scattering to the Local Mixture Strength Measurements in SI Engine during Intake Stroke," SAE Paper 872151, 1987.
26. Kadota, T., Satoh, T., Memon, M. A., and Sumida, O., "Mixture Strength Measurements in the Combustion Chamber of SI Engine via Rayleigh Scattering," JSME (Int'l) Journal, Series II, Vol. 32, No. 1, pp. 134 - 141, 1989.
27. Kadota, T., Zhao, F.-Q., and Miyoshi, K., "Rayleigh Scattering Measurements of Transient Fuel Vapor Concentration in a Motored Spark Ignition Engine," SAE Paper 900481, 1990.
28. Zhao, F.-Q., Kadota, T., and Takemoto, T., "Temporal and Cyclic Fluctuation of Fuel Vapor Concentration in a Spark Ignition Engine," SAE Paper 912346, 1991.
29. Baritaud, T. A., and Heinze, T. A., "Gasoline Distribution Measurements with PLIF in a SI Engine," SAE Paper 922355, 1992
30. Maly, R. R., et al., "Quantitative 2D LIF Measurements of Air/Fuel Ratios During the Intake Stroke in a Transparent SI Engine," SAE Paper 922320, 1992.
31. Shimizu, R., et al., "Measurement of Air-Fuel Mixture Distribution in a Gasoline Engine Using LIEF Technique," SAE Paper 922356, 1992.
32. Videto, B. D., and Santavicca, D. A., "A Turbulent Flow System for Studying Turbulent Combustion Processes," Combust. Sci. and Tech., Vol. 76, pp. 159-164, 1991.
33. Eckbreth, A. C., "Laser Diagnostics for Combustion, Temperature and Species," Energy and Engg. Science Series, Ed. by Gupta, A. K. and Lilley, D. G., The Abacus Press, 1988.
34. Tennekes, H. and Lumley, J.L., A First Course In Turbulence, The MIT Press, 1972.
35. Huntzinger, G. O., and Rigsby, G. E., "HEI - A New Ignition System Through New Technology," SAE Paper 750346, 1975.
36. Gordon, S., and McBride, B. J., "Computer Program for Calculation of Complex Chemical Equilibrium Compositions, Rocket Performance, Incident and Reflected Shocks, and Chapman-Jouguet Detonations," NASA SP-273, 1986.
37. Metghalchi, M., and Keck, J. C., "Burning Velocities of Mixtures of Air with Methanol, Isooctane, and Indolene at High Pressure and Temperature," Combustion and Flame, Vol. 48, pp. 191-210, 1982.
38. Ryan, T. W., III, and Lestz, S. S., "The Laminar Burning Velocity of Isooctane, N-Heptane, Methanol, Methane, and Propane at Elevated Temperature and Pressures in the Presence of a Diluent," SAE Paper 800103, 1980.
39. Blint, R. J., "Flammability Limits for Exhaust Gas Diluted Flames," GM Research Publication, GMR-6036, 1988.
40. Metghalchi, M., and Keck, J. C., "Laminar Burning Velocity of Propane-Air Mixtures at High Temperature and Pressure," Combustion and Flame, Vol. 38, pp. 143-154, 1980.
41. Law, C. K., "Dynamics of Stretched Flames," 22nd Symposium (Int'l) on Combustion, pp. 1381-1402, 1988.
42. Palm-Leis, A., and Strehlow, R. A., "On the Propagation of Turbulent Flames," Combustion and Flame, Vol.

13, pp. 111-129, 1969.
43. Strehlow, R. A., Combustion Fundamentals, McGraw-Hill, 1984.
44. Law, C. K., "A Compilation of Experimental Data on Laminar Burning Velocities," 1992.
45. Weaver, C. E. and Santavicca, D. A., "Correlation of Cycle-Resolved Flame Kernel Growth and Cylinder Pressure in an Optically-Accessible Engine," SAE Paper 922171, 1992.
46. Witze, P. O., Hall, M. J. and Bennet, M. J., "Cycle-Resolved Measurements of Flame Kernel Growth and Motion Correlated with Combustion Duration," SAE Paper 900023, 1990.
47. Glassman, I., Combustion, 2nd Ed., Academic Press, Inc., 1987.
48. Daneshyar, H., and Hill, P. G., "The Structure of Small Scale Turbulence and Its Effect on Combustion in Spark Ignition Engines," Prog. Energy Combust. Sci., Vol. 13, pp.47-73, 1987.
49. Bradley, D., Hynes, J., Lawes, M., and Sheppard, C. G. W., "Limitations to Turbulence-Enhanced Burning Rates in Lean Burn Engines," Proc. of the Inst. of Mech. Engr., International Conference, 1988.
50. Hall, M. J., and Bracco, F. V., "A Study of Velocities and Turbulence Intensities Measured in Firing and Motored Engines," SAE Paper 870453, 1987.
51. Baritaud, T. A.,"Combustion and Fluid Dynamic Measurements in a Spark Ignition Engine: Effects of Thermochemistry and Velocity Field; Turbulent Flame Speeds," SAE Paper 892098, 1989.
52. Smith, J. R., "The Influence of Turbulence on Flame Structure in an Engine," A.S.M.E. Conf., Phoenix, Arizona, Nov. 14-19, 1982.
53. Witze, P. O., and Vilchis, F. R., "Stroboscopic Laser Shadowgraphy Study of the Effect of Swirl on Homogeneous Combustion in a Spark-Ignition Engine," SAE Paper 810226, 1981.

DATE
FILMED
7/25/94
END